Proximity magnetoresistance in graphene induced by magnetic insulators

D. A. Solis,[1] A. Hallal,[1] X. Waintal,[2] and M. Chshiev[1]
[1]*Univ. Grenoble Alpes, CEA, CNRS, Spintec, 38000 Grenoble, France*
[2]*Univ. Grenoble Alpes, CEA, IRIG, Pheliqs, 38000 Grenoble, France*

(Received 19 July 2018; revised manuscript received 5 June 2019; published 3 September 2019)

We demonstrate the existence of the giant proximity magnetoresistance (PMR) effect in a graphene spin valve where spin polarization is induced by a nearby magnetic insulator. PMR calculations were performed for yttrium iron garnet (YIG), cobalt ferrite (CFO), and two europium chalcogenides EuO and EuS. We find significant PMR (up to 100%) values defined as a relative change of graphene conductance with respect to parallel and antiparallel alignment of two proximity-induced magnetic regions within graphene. Namely, for high Curie temperature (T_C) CFO and YIG insulators, which are particularly important for applications, we obtain 22% and 77% at room temperature, respectively. For low T_C chalcogenides, EuO and EuS, the PMR is 100% in both cases. Furthermore, the PMR is robust with respect to system dimensions and edge-type termination, and it even maintains significant values (around 50% for YIG) in the presence of considerable spin-orbit coupling strength. Our findings show that it is possible to induce spin-polarized currents in graphene with no direct injection through magnetic materials.

DOI: 10.1103/PhysRevB.100.104402

I. INTRODUCTION

Graphene is a two-dimensional (2D) material [1,2] that has attracted a lot of interest in view of its unique physical properties and potential applications in diverse fields such as electronics, spintronics, valleytronics, and quantum computing [3–6]. Due to its weak spin-orbit coupling (SOC) [7–16], graphene possesses a long spin relaxation time and lengths even at room temperature [17]. Yet, inducing SOC is essential to manipulate spin current in graphene. A huge SOC in graphene can be induced by adding adatoms [18] or using 2D substrates [19] such as metals [20,21], transition-metal dichalcogenides [22–24], or topological insulators [25–27]. While all of these properties offer an optimal platform for spin manipulation, finding ways to control SOC while keeping the efficiency and robustness of spin polarization at room temperature remains a challenge.

Several methods have been proposed in order to introduce ferromagnetic order in graphene, including functionalization with adatoms [28], the addition of defects [29,30], and by means of the proximity effect via an adjacent ferromagnet [31–36]. The latter approach attracted a lot of interest using magnetic insulators (MIs) as a substrate to induce exchange splitting in graphene. When a material is placed on top of a magnetic insulator, it can acquire proximity-induced spin polarization and exchange splitting [31] resulting from the hybridization between p_z orbitals and those of the neighboring magnetic insulator. For practical purposes, the implementation in spintronic devices of this kind of material could lead to lower power consumption because, unlike traditional spin-injection techniques, no current injection across an adjacent ferromagnet (FM) is required. Experimentally, the existence of proximity exchange splitting via a magnetic insulator in graphene has been demonstrated with exchange fields up to 100 T using the coupling between graphene and EuS [34]. For a yttrium iron garnet/graphene (YIG/Gr)-based system, using nonlocal spin transport measurements, Leutenantsmeyer *et al.* [35] demonstrated an exchange field strength of 0.2 T. Another possibility of inducing exchange splitting in graphene using FM metal by separating them using an alternative 2D material such as hexa-boron nitride (hBN) was also proposed theoretically [32].

Recent studies have suggested the creation of graphene-based devices where an EuO-graphene junction can act as a spin filter and spin valve simultaneously by gating the system [37]. It was also demonstrated [38] that a double EuO barrier on top of a graphene strip can exhibit negative differential resistance, making this system a spin-selective diode. However, the drawback of using EuO is its low Curie temperature and the predicted strong electron doping [31]. It was proposed, therefore, to use high Curie temperature materials such as YIG or cobalt ferrite (CFO) [39]. Indeed, a large change in the resistance of a graphene-based spintronic device has been reported recently where the heavy doping induced by YIG could be treated by gating [40]. Alternative concepts were also proposed based on exploration of the spin-dependent tunneling effect or valley-polarized currents in graphene monolayer modulated by magnetic barriers created by FM stripes across a dielectric layer or a graphene strain [41,42].

In this paper, we demonstrate the existence of the proximity magnetoresistance (PMR) effect in graphene for four different MIs: YIG, CFO, europium oxide (EuO), and europium sulfide (EuS). Using *ab initio* parameters reported in Ref. [39], we show that for YIG- and CFO-based lateral graphene-based devices with armchair edges, PMR values could reach 77% and 22% at room temperature (RT), respectively. With chalcogenides EuS and EuO, PMR values can reach 100% at 16 and 70 K, respectively. In addition, we demonstrate the robustness of this effect with respect to system dimensions and edge-type termination. Furthermore, we explore the impact of SOC and find that it does not significantly affect the PMR.

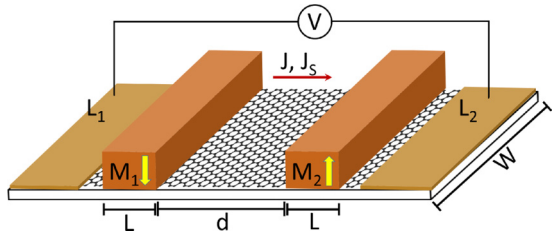

FIG. 1. Lateral spintronic device comprising two magnetic insulators on top of a graphene sheet. The magnetic graphene regions have a length L, width W, and they are separated by a distance d.

These findings will stimulate experimental investigations of the proposed phenomenon of PMR and the development of other proximity-effect-based spintronic devices.

II. METHODOLOGY

To calculate conductances and PMR, we employed the tight-binding approach with the scattering matrix formalism conveniently implemented within the KWANT package [43]. The system modeled is shown in Fig. 1 and comprises two identical proximity-induced magnetic regions of width W and length L resulting from insulators with magnetizations $\mathbf{M}_1$ and $\mathbf{M}_2$, separated by a distance d of the nonmagnetic region of a graphene sheet with armchair edges. Both magnetic graphene regions are separated from the leads L_1 and L_2 by a small pure graphene region. Note that alternative concepts based on similar geometries have been proposed where the current could be controlled via gating [37,38,40,41] or strain [42]. For instance, adding a dielectric between graphene and FM stripes can be done to explore spin-dependent tunneling magnetoresistance in such devices via the creation of magnetic barriers using Klein tunneling [41]. Here, we exploit the magnetic insulator proximity effect in order to control spin-dependent transport within graphene in more simple geometry.

To take into account the magnetism arising in graphene from the proximity effects induced by the MIs, we use in the Hamiltonian the parameters obtained for different MIs in Ref. [39]. It is important to note that the magnetic regions do not affect the linear dispersion of graphene bands except for breaking the valley and electron-hole symmetry, resulting in spin-dependent band splitting and doping. The discretized Hamiltonian for the magnetic graphene regions can be expressed as

$$\begin{aligned} H = & \sum_{i\sigma}\sum_{l} t_{l\sigma} c^{\dagger}_{(i+l)1\sigma} c_{i0\sigma} + \text{H.c.} \\ & + \sum_{i\sigma\sigma'}\sum_{\mu=0}^{1} [\delta + (-1)^{\mu}\Delta_{\delta}] c^{\dagger}_{i\mu\sigma} [\vec{m}\cdot\vec{\sigma}] c_{i\mu\sigma'} \\ & + \sum_{i\sigma}\sum_{\mu=0}^{1} [E_D + (-1)^{\mu}\Delta_s] c^{\dagger}_{i\mu\sigma} c_{i\mu\sigma}, \end{aligned} \tag{1}$$

where $c^{\dagger}_{i\mu\sigma}$ ($c^{\dagger}_{i\mu\sigma}$) creates (annihilates) an electron of type $\mu = 0$ for A sites and $\mu = 1$ for B sites on the unit cell i with spin $\sigma = \uparrow (\downarrow)$ for up (down) electrons. $\vec{m}$ and $\vec{\sigma}$, respectively, represent a unit vector that points in the direction of the magnetization and the vector of Pauli matrices, so that $\vec{m}\cdot\vec{\sigma} = m_x\sigma_x + m_y\sigma_y + m_z\sigma_z$. The anisotropic hopping $t_{l\sigma}$ connects unit cells i to their nearest-neighbor cells $i + l$. Parameters δ, Δ_{δ}, and Δ_s are defined via exchange spin-splittings δ_e (δ_h) of the electrons (holes) and spin-dependent band gaps Δ_{σ} defined in Ref. [39]. E_D indicates the Dirac cone position with respect to the Fermi level. The Hamiltonian for the whole device is obtained by making the aforementioned parameters spatially dependent.

TABLE I. Hopping parameters used in Eq. (1) for each magnetic insulator considered.

Material	Hopping direction	Spin-up (eV)	Spin-down (eV)
YIG	t	3.6	3.8
CFO	t_1	1.38	1.44
	t_2	$1.41e^{-i0.01}$	$1.48e^{-i0.01}$
	t_3	$1.36e^{-i0.02}$	$1.44e^{-i0.02}$
EuS	t	4.5	4.8
EuO	t	4.9	4.3

To obtain hopping parameters of Hamiltonian (1), we fitted tight-binding bands to those obtained from first-principles calculations in Ref. [39]. The results of the fitting procedure in the case of graphene magnetized by YIG, CFO, EuS, and EuO are shown in Figs. 2(a), 2(b) 2(c), and 2(d), respectively. The corresponding hopping parameters are given in Table I. As one can see, the graphene bands obtained with the tight-binding Hamiltonian given by Eq. (1) are in good agreement with those obtained using density functional theory (DFT), confirming the suitability of our model for transport calculations. Note that due to the presence of superficial tension at the interface between CFO and graphene, hopping parameters in this case are anisotropic, as they depend on the direction to the nearest neighbor as specified in the inset of Fig. 2(b).

The conductance for parallel and antiparallel configurations of magnetizations $\mathbf{M}_1$ and $\mathbf{M}_2$ in the linear-response regime is then obtained according to

$$G_{\mathrm{P(AP)}} = \frac{e}{h}\sum_{\sigma}\int T^{\sigma}_{\mathrm{P(AP)}}\left(\frac{-\partial f}{\partial E}\right) dE, \tag{2}$$

where $T^{\sigma}_{\mathrm{P(AP)}}$ indicates the spin-dependent transmission probability for parallel (antiparallel) magnetization configurations, and $f = 1/(e^{(E-\mu)/k_BT} + 1)$ represents the Fermi-Dirac distribution, with μ and T being the electrochemical potential (Fermi level) and the temperature, respectively. It is important to note that temperature smearing has been taken into account using the Curie temperature of each MI.

The PMR amplitude has been defined according to the following expression:

$$\mathrm{PMR} = \left(\frac{G_{\mathrm{P}} - G_{\mathrm{AP}}}{G_{\mathrm{P}} + G_{\mathrm{AP}}}\right) \times 100\%. \tag{3}$$

To determine the impact of the system dimensions on the PMR, several calculations were carried out for different lengths, widths, and separations of the magnetic regions. Furthermore, we checked the robustness of PMR on the edge-type termination by calculating the PMR for systems with zigzag, armchair, and rough edges. The latter were created

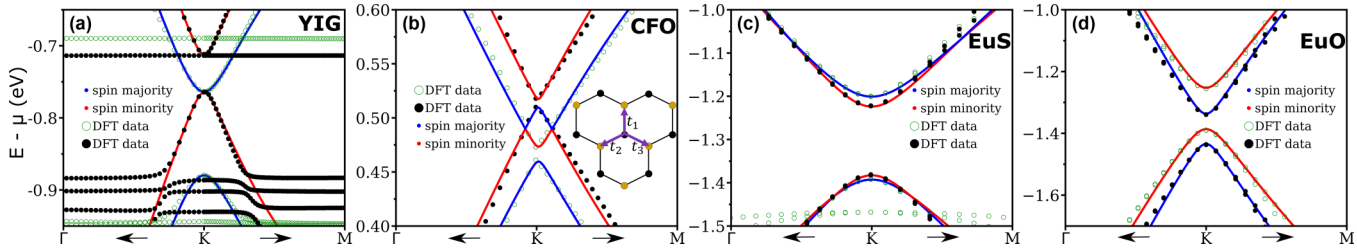

FIG. 2. Band structure obtained using the tight-binding Hamiltonian defined by Eq. (1) (solid lines) fitted to the band structure from DFT spin-majority (green open circles) and spin-minority (black filled circles) data for the cases with (a) YIG, (b) CFO, (c) EuS, and (d) EuO from Ref. [39]. The inset in (b) shows the anisotropic hoppings reported in Table I.

by removing atoms and bounds randomly and deleting the dangling atoms at the new edges.

III. RESULTS AND DISCUSSION

In Fig. 3 we present the PMR curves for lateral device structures based on YIG, CFO, EuS, and EuO on top of a graphene sheet with armchair edges. Taking into account Curie temperatures for these materials, the curves were smeared out using 16 K (70 K) for EuS (EuO), and 300 K for YIG and CFO. For a system with YIG we found a maximum PMR value of 77%, while for CFO the value obtained was 22%. When the chalcogenides EuS and EuO are used, the maximum PMR values reach 100%. Among the materials studied, YIG represents the most suitable candidate for lateral spintronic applications due to both high Curie temperature and a considerably large PMR value.

To elucidate the underlying physics behind these PMR results, let us analyze the details of the conductance behavior. In Figs. 4(a) and 4(b) we reproduce the graphene bands in proximity to YIG and the corresponding transmission probabilities resolved in spin for P and AP configurations at $T = 0$ K for a system with dimensions $L = 49.2$ nm, $W = 39.6$ nm, and $d = 1.5$ nm. One can see that for energies between -0.88 and -0.78 eV there is no majority-spin state

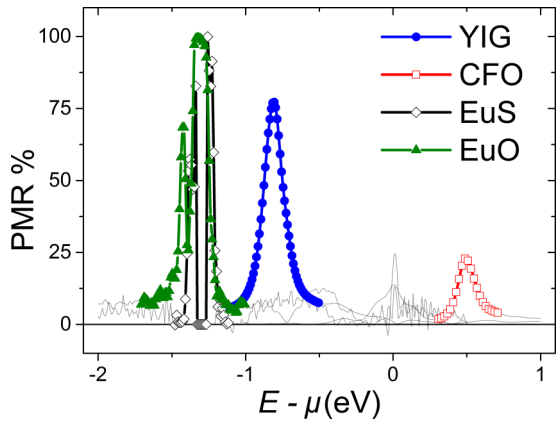

FIG. 3. Proximity magnetoresistance defined by Eq. (3) as a function of energy with respect to the Fermi level for YIG (blue circles), CFO (red squares), EuS (black diamonds), and EuO (green triangles) using temperature smeared conductances at $T = 300$, 300, 16, and 70 K, respectively. System dimensions are $L = 49.2$ nm, $W = 39.6$ nm, and $d = 1.5$ nm.

present and the only contribution to transmission $T_P^{\downarrow}$ is from the minority-spin channel [Fig. 4(b), red solid line]. In other words, the situation within this energy range is half-metallic giving rise to maximum PMR values of 100% using the "pessimistic" definition given by Eq. (3). A similar situation exists for energy ranges between -0.72 and -0.75 eV, but this time the only contribution $T_P^{\uparrow}$ is from the majority-spin channel [Fig. 4(b), red dashed line]. One should point out here that the conduction profile is obtained by combining both the magnetic and nonmagnetic regions into one scattering region. The conductance of a pure graphene nanoribbon sheet represents quantized steps due to transverse confinement with no conductivity at zero energy depending on its edges. Inducing magnetism within the graphene sheet leads to symmetry breaking with the shift of exchange split gaps in the vicinity of the Dirac cone region below the Fermi level. This leads to a characteristic conductance profile with two minima at around -0.8 and 0 eV (not shown here) due to the Dirac cone regions of magnetized and pure graphene. The corresponding conductances for the parallel (G_P) and antiparallel (G_{AP}) magnetic configurations at $T = 300$ K are shown in Fig. 4(c). Interestingly, even at room temperature the PMR for YIG-based structure preserves a very high value of about 77%, as was already pointed out , a behavior that is very encouraging for future experiments on PMR. As a guide to the eye, dashed lines highlight the energy value where the PMR has a maximum in Fig. 4.

Since the edges may strongly influence the aforementioned properties of the system, we next explore the robustness of PMR against different edge types of the graphene channel of the proposed device. It is well known that an electric field can trigger half-metallicity in zigzag nanoribbons due to the antiferromagnetic interaction of the edges [44]. On the other hand, graphene nanoribbons with armchair edges can display insulating or metallic behavior depending on the graphene nanoribbon (GNR) width [45,46]. Armchair and zigzag edges are particular cases and the most symmetric edge directions in graphene. But one can cut GNR at an intermediate angular direction between these two limiting cases, giving rise to an intermediate direction characterized by a chirality angle θ [47]. Graphene band structure is highly dependent on θ. When the angle is increased, the length of the edge states localized at the Fermi level decreases and eventually disappears in the limiting case when $\theta = 30^{\circ}$, i.e., when it acquires an armchair edge. In the laboratory conditions, graphene sheets are finite and have imperfections that influence their transport

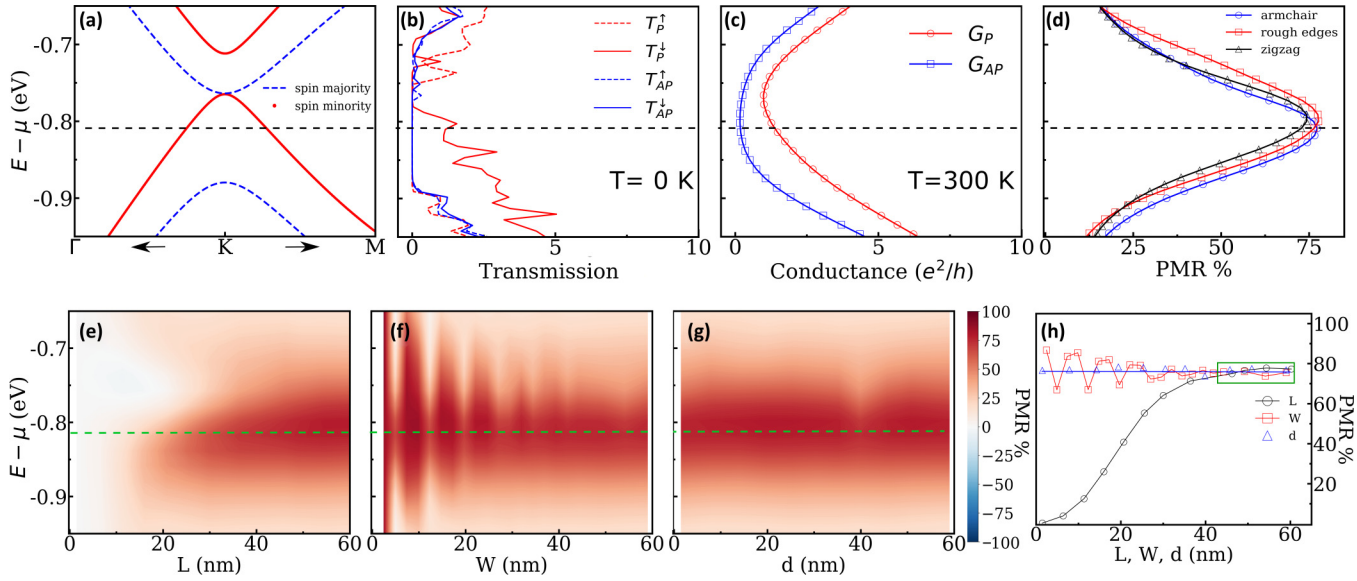

FIG. 4. (a) Band structure reproduced using the DFT parameters from Ref. [39] for graphene in proximity to YIG. (b) Transmission probabilities for majority (dashed lines) and minority (solid) spin channel for parallel (red) and antiparallel (blue) magnetization configurations at $T = 0$ K for a system with dimensions $L = 49.2$ nm, $W = 39.6$ nm, and $d = 1.5$ nm. (c) Resulting conductance for parallel (red circles) and antiparallel (blue squares) magnetization configurations at 300 K. (d) PMR for a device with armchair (blue circles), rough (red squares), and zigzag (black triangles) edge termination of graphene. PMR profiles as a function of (e) L, (f) W, and (g) d for a system with armchair edges. (h) Dependence of PMR for the energy outlined by a dashed line in (e), (f), and (g) as a function of L (black circles), W (red squares), and d (blue triangles). The green square highlights the region where PMR becomes independent of system dimensions.

properties. For defects at the edges, it has been demonstrated that rough edges can diminish the conductance of a graphene nanoribbon, as was shown in Ref. [48], or it may exhibit a nonzero spin conductance as reported in Ref. [49].

To demonstrate the robustness of PMR with respect to the edge type, we thus performed calculations with the same system setup (Fig. 1) but this time for various edge terminations. The resulting PMR behavior for the cases with armchair, rough, and zigzag edges is shown in Fig. 4(d). The former have been modeled by creating extended vacancies distributed randomly. It is clear that the maximum PMR value does not present a significant variation, maintaining for all cases PMR values around 75%. With this result at hand, we can claim that the PMR is indeed robust with respect to edge termination type.

As a next step, we checked the dependence of the PMR on different system dimensions, i.e., the length of the magnetic region L, the system width W, and the separation between the magnetic regions d. The corresponding dependences for a system with armchair edges are presented, respectively, in Figs. 4(e), 4(f) and 4(g). One can see that for all energy ranges, the PMR ratio has a tendency to increase as a function of L, approaching a limiting value of 77% at energies around -0.81 eV [indicated by a dashed line Fig. 4(e)]. As for the dependence of the PMR as a function of GNR width W, clear oscillations are present with a tendency to vanish as the system widens [Fig. 4(f)]. These oscillations depend on edge termination type, and they are more pronounced for a system with armchair edges compared to zigzag or rough edges (not shown). On the contrary, the PMR shows almost constant behavior as a function of separation between the magnets d [Fig. 4(g)] due to the fact that transport is in a ballistic regime. For convenience, we summarize all these dependencies in Fig. 4(h) at an energy -0.81 eV as a function of L, W, and d. One can clearly see that the PMR saturates as the system dimensions are increased. At the same time, it shows the oscillations in the PMR for small W as well as the invariance of the PMR with respect to d. For large dimensions [highlighted by the green box in Fig. 4(h)], we can claim that the PMR is indeed robust, and the maximum PMR value would eventually be limited only by the magnitude of the spin diffusion length in the system.

Finally, we consider the impact of spin-orbit coupling on the PMR. Despite weak SOC within graphene, the proximity of adjacent materials can induce the interfacial Rashba SOC [8]. Actually, this phenomenon became very important in two-dimensional systems because it allows for efficient spin manipulation and it provides a versatile way to generate, control, and convert spin currents [50]. Different materials have been considered, therefore, to enhance SOC strength in graphene, including metals [20,21], transition-metal dichalcogenides [22–24,51], and topological insulators [25–27]. Of particular interest in our case is the use of YIG due to its high Curie temperature, where proximity-induced ferromagnetism with an enhanced SOC parameter $\lambda_R < 12$ meV has been recently reported [33].

In our tight-binding approach, the Rashba SOC is included by adding the following term:

$$H_{\mathrm{SO}} = i\lambda_R \sum_{i\sigma\sigma'} \sum_{l} c^{\dagger}_{(i+l)1\sigma} \left[\sigma^{x}_{\sigma\sigma'} d^{x}_{l} - \sigma^{y}_{\sigma\sigma'} d^{y}_{l}\right] c_{i0\sigma'} + \mathrm{H.c.}, \tag{4}$$

where the vector $\vec{d}_l = (d^x_l, d^y_l)$ connects the two nearest neighbors, and λ_R indicates the SOC strength. The values of λ_R

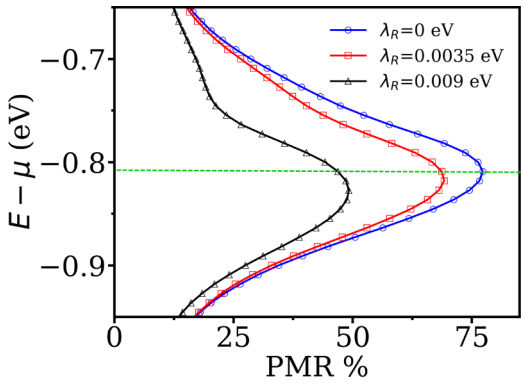

FIG. 5. PMR dependencies for three values of Rashba spin-orbit interaction parameter λ_R defined by Eq. (4) for the YIG-based system with armchair edges and of dimensions $L = 49.2$ nm, $W = 39.6$ nm, and $d = 1.5$ nm. The dashed line is a guide to the eye that shows the maximum value when $\lambda_R = 0$ eV.

are generally in the range between 1 and 10 meV (see, for instance, Ref. [52]). Keeping this in mind, we present in Fig. 5 the PMR dependences for three values of Rashba SOC. One can see that increasing the strength of SOC λ_R lowers the PMR. This behavior is expected and could be attributed to the fact that the spin-orbit interaction mixes the spin channels. These dependencies allow us to conclude that PMR is also quite robust against SOC, and even in the worst-case scenario it remains of the order of 50% (cf. the black triangles and blue circles in Fig. 5).

IV. CONCLUSIONS

In this paper, we introduced the proximity-induced magnetoresistance phenomenon in a graphene-based lateral system comprising regions with proximity-induced magnetism by four different magnetic insulators. For YIG- and CFO-based devices, we found PMR ratios of 77% and 22% at room temperature, respectively. For chalcogenide-based systems, i.e., with EuS and EuO, we found PMR values of 100% for both at 16 and 70 K, respectively. Very importantly, it is demonstrated that the PMR is robust with respect to system dimensions and edge-type termination. Furthermore, the PMR survives in case of the presence of SOC decreasing only by about half even in the case of considerably big SOC strength values. We hope this work will encourage further experimental research and will be useful for the development of novel generation of spintronic devices based on generation and exploring spin currents without passing charge currents across ferromagnets.

ACKNOWLEDGMENTS

We thank J. Fabian and S. Roche for fruitful discussions. This project has received funding from the European Union's Horizon 2020 research and innovation programme under Grant Agreements No. 696656 and No. 785219 (Graphene Flagship). X.W. acknowledges support by ANR Project Gransport (ANR-17-GRF1-0004).

[1] K. S. Novoselov, A. K. Geim, S. V. Morozov, D. Jiang, M. I. Katsnelson, I. V. Grigorieva, S. V. Dubonos, and A. A. Firsov, Nature (London) **438**, 197 (2005).
[2] Y. Zhang, H. L. S. Yan-Wen Tan, and P. Kim, Nature (London) **438**, 201 (2005).
[3] A. H. Castro Neto, F. Guinea, N. M. R. Peres, K. S. Novoselov, and A. K. Geim, Rev. Mod. Phys. **81**, 109 (2009).
[4] S. Roche, J. Åkerman, B. Beschoten, J.-C. Charlier, M. Chshiev, S. P. Dash, B. Dlubak, J. Fabian, A. Fert, M. Guimarães, F. Guinea, I. Grigorieva, C. Schönenberger, P. Seneor, C. Stampfer, S. O. Valenzuela, X. Waintal, and B. van Wees, 2D Mater. **2**, 030202 (2015).
[5] S. A. Vitale, D. Nezich, J. O. Varghese, P. Kim, N. Gedik, P. Jarillo-Herrero, D. Xiao, and M. Rothschild, Small **14**, 1801483 (2018).
[6] D. L. Björn Trauzettel, D. V. Bulaev and G. Burkard, Nat. Phys. **3**, 192 (2007).
[7] N. Tombros, C. Jozsa, M. Popinciuc, H. T. Jonkman, and B. J. van Wees, Nature (London) **448**, 571 (2007).
[8] W.-K. Tse, Z. Qiao, Y. Yao, A. H. MacDonald, and Q. Niu, Phys. Rev. B **83**, 155447 (2011).
[9] M. Popinciuc, C. Józsa, P. J. Zomer, N. Tombros, A. Veligura, H. T. Jonkman, and B. J. van Wees, Phys. Rev. B **80**, 214427 (2009).
[10] B. Dlubak, P. Seneor, A. Anane, C. Barraud, C. Deranlot, D. Deneuve, B. Servet, R. Mattana, F. Petroff, and A. Fert, Appl. Phys. Lett. **97**, 092502 (2010).
[11] W. Han and R. K. Kawakami, Phys. Rev. Lett. **107**, 047207 (2011).
[12] T.-Y. Yang, J. Balakrishnan, F. Volmer, A. Avsar, M. Jaiswal, J. Samm, S. R. Ali, A. Pachoud, M. Zeng, M. Popinciuc, G. Güntherodt, B. Beschoten, and B. Özyilmaz, Phys. Rev. Lett. **107**, 047206 (2011).
[13] T. Maassen, J. J. van den Berg, N. Ijbema, F. Fromm, T. Seyller, R. Yakimova, and B. J. van Wees, Nano Lett. **12**, 1498 (2012).
[14] B. Dlubak, M.-B. Martin, C. Deranlot, B. Servet, S. Xavier, R. Mattana, M. Sprinkle, C. Berger, W. A. De Heer, F. Petroff, A. Anane, P. Seneor, and A. Fert, Nat. Phys. **8**, 557 (2012).
[15] A. W. Cummings and S. Roche, Phys. Rev. Lett. **116**, 086602 (2016).
[16] D. Van Tuan, F. Ortmann, A. W. Cummings, D. Soriano, and S. Roche, Sci. Rep. **6**, 21046 (2016).
[17] M. Drögeler, C. Franzen, F. Volmer, T. Pohlmann, L. Banszerus, M. Wolter, K. Watanabe, T. Taniguchi, C. Stampfer, and B. Beschoten, Nano Lett. **16**, 3533 (2016).
[18] J. Balakrishnan, G. Kok Wai Koon, M. Jaiswal, A. H. Castro Neto, and B. Özyilmaz, Nat. Phys. **9**, 284 (2013).
[19] I. Žutić, A. Matos-Abiague, B. Scharf, H. Dery, and K. Belashchenko, Mater. Today **22**, 85 (2019).
[20] I. I. Klimovskikh, M. M. Otrokov, V. Y. Voroshnin, D. Sostina, L. Petaccia, G. Di Santo, S. Thakur, E. V. Chulkov, and A. M. Shikin, ACS Nano **11**, 368 (2017).
[21] J. Slawińska and J. I. Cerdá, New J. Phys. **21**, 073018 (2019).

[22] A. Avsar, J. Y. Tan, T. Taychatanapat, J. Balakrishnan, G. K. W. Koon, Y. Yeo, J. Lahiri, A. Carvalho, A. S. Rodin, E. C. T. O'Farrell, G. Eda, A. H. Castro Neto, and B. Özyilmaz, Nat. Commun. **5**, 4875 (2014).
[23] Z. Wang, D.-K. Ki, H. Chen, H. Berger, A. H. MacDonald, and A. F. Morpurgo, Nat. Commun. **6**, 8339 (2015).
[24] M. Gmitra, D. Kochan, P. Högl, and J. Fabian, Phys. Rev. B **93**, 155104 (2016).
[25] K.-H. Jin and S.-H. Jhi, Phys. Rev. B **87**, 075442 (2013).
[26] P. Lee, K.-H. Jin, S. J. Sung, J. G. Kim, M.-T. Ryu, H.-M. Park, S.-H. Jhi, N. Kim, Y. Kim, S. U. Yu, K. S. Kim, D. Y. Noh, and J. Chung, ACS Nano **9**, 10861 (2015).
[27] J. Zhang, C. Triola, and E. Rossi, Phys. Rev. Lett. **112**, 096802 (2014).
[28] A. J. M. Giesbers, K. Uhlířová, M. Konečný, E. C. Peters, M. Burghard, J. Aarts, and C. F. J. Flipse, Phys. Rev. Lett. **111**, 166101 (2013).
[29] O. V. Yazyev and L. Helm, Phys. Rev. B **75**, 125408 (2007).
[30] H.-X. Yang, M. Chshiev, D. W. Boukhvalov, X. Waintal, and S. Roche, Phys. Rev. B **84**, 214404 (2011).
[31] H. X. Yang, A. Hallal, D. Terrade, X. Waintal, S. Roche, and M. Chshiev, Phys. Rev. Lett. **110**, 046603 (2013).
[32] K. Zollner, M. Gmitra, T. Frank, and J. Fabian, Phys. Rev. B **94**, 155441 (2016).
[33] Z. Wang, C. Tang, R. Sachs, Y. Barlas, and J. Shi, Phys. Rev. Lett. **114**, 016603 (2015).
[34] P. Wei, S. Lee, F. Lemaitre, L. Pinel, D. Cutaia, W. Cha, F. Katmis, Y. Zhu, D. Heiman, J. Hone, J. S. Moodera, and C.-T. Chen, Nat. Mater. **15**, 711 (2016).
[35] J. C. Leutenantsmeyer, A. A. Kaverzin, M. Wojtaszek, and B. J. van Wees, 2D Mater. **4**, 1 (2016).
[36] H. Haugen, D. Huertas-Hernando, and A. Brataas, Phys. Rev. B **77**, 115406 (2008).
[37] Y. Song and G. Dai, Appl. Phys. Lett. **106**, 223104 (2015).
[38] Y. Song, Y. Liu, X. Feng, F. Yan, and W. Zhang, Phys. Chem. Chem. Phys. **20**, 1560 (2018).
[39] A. Hallal, F. Ibrahim, H. Yang, S. Roche, and M. Chshiev, 2D Mater. **4**, 025074 (2017).
[40] Y. Song, J. Phys. D **51**, 025002 (2017).
[41] F. Zhai and K. Chang, Phys. Rev. B **77**, 113409 (2008).
[42] F. Zhai, X. Zhao, K. Chang, and H. Q. Xu, Phys. Rev. B **82**, 115442 (2010).
[43] C. W. Groth, M. Wimmer, A. R. Akhmerov, and X. Waintal, New J. Phys. **16**, 063065 (2014).
[44] Y.-W. Son, M. L. Cohen, and S. G. Louie, Nat. Phys. **444**, 347 (2007).
[45] K. Nakada, M. Fujita, G. Dresselhaus, and M. S. Dresselhaus, Phys. Rev. B **54**, 17954 (1996).
[46] A. Kimouche, M. M. Ervasti, R. Drost, S. Halonen, P. M. Harju, A. Joensuu, J. Sainio, and P. Liljeroth, Nat. Commun. **6**, 10177 (2015).
[47] O. V. Yazyev, Acc. Chem. Res. **46**, 2319 (2013).
[48] F. Libisch, S. Rotter, and J. Burgdörfer, New J. Phys. **14**, 123006 (2012).
[49] M. Wimmer, I. Adagideli, S. Berber, D. Tománek, and K. Richter, Phys. Rev. Lett. **100**, 177207 (2008).
[50] J. Varignon, L. Vila, A. Barthélémy, and M. Bibes, Nat. Phys. **14**, 322 (2018).
[51] T. S. Ghiasi, J. Ingla-Aynés, A. A. Kaverzin, and B. J. van Wees, Nano Lett. **17**, 7528 (2017).
[52] Z. Qiao, W. Ren, H. Chen, L. Bellaiche, Z. Zhang, A. H. MacDonald, and Q. Niu, Phys. Rev. Lett. **112**, 116404 (2014).